 doi:10.20944/preprints202206.0051.v1

Article

Study of Buried Basin in Copernicus Area Based on Multi Source Remote Sensing Data

Xiaojian Xu[1,2,3], Zhizhong Kang[1,2,3], Teng Hu[1,2,3,*], Xing Du[1,2,3], Lin Zhao[1,2,3]

[1] School of Land Science and Technology, China University of Geosciences (Beijing), Beijing, China; 3012210002@email.cugb.edu.cn (X.X.); zzkang@cugb.edu.cn (Z.K.); huteng@cugb.edu.cn (T.H.); 20122200005@cugb.edu.cn (X.D.); linzhao1020@163.com (L.Z.)
[2] Research Center of Lunar and Planetary Remote Sensing Exploration, China University of Geosciences (Beijing), Beijing, China;
[3] Subcenter of International Cooperation and Research on Lunar and Planetary Exploration, Center of Space Exploration, Ministry of Education of the People's Republic of China, Beijing, China;
[*] Correspondence: zzkang@cugb.edu.cn

Abstract: Masons are often overlooked part of impact basins, but play an important role in revealing the lunar history. Previous study in masons were usually limited to gravity data. Few researches were reported on morphology features and chronology, which hampers the construction of a complete geological interpretation for the evolution of each mascons. We use multi source remote sensing data to identify the details characteristic of mascons. Result of topography, gravity and characteristic are combined to prove that a mason beside Copernicus crater is a buried peak-ring basin which is about 130km and 260km in diameter. The underground structure is of confirmed as 890m thick mare basalts by analyzing the spectral feature of the material in a geological outcrop called Copernicus H. Geology evolution analysis joint crater size-frequency distribution (CSDF) dating demonstrate that the buried basin impact event occurred in 3.6Ga. Then a hawaiian-style eruption in late Imbrian formed Sinus Aestuum Ⅰ Dark Mantling Deposit (DMD). Mare basalts filling in 3.4Ga. After that, ejecta from Copernicus impact event in about 820Ma and weathering processes cause the disappearing from lunar surface of the buried basin.

Keywords: Copernicus; buried basin; mascons; multi source remote sensing data; planetary geology; planetary topography; geomorphology

1. Introduction

Plenty of various data have been gathered over a half-century of lunar exploration. Include images, topography, spectrum, gravity, magnetism and so on. Combine multi source data experimental results help scientists to learn the general process instead of part view of planetary geology evolution. Craters are among the most noticeable geomorphological unit on the planetary surface. Most recent studies focus on their morphological characteristics and spatial distributions [1]. However, researches based on multi source data can revise geologic framework more accurately. For example, repetitive lava filling events in Sinus Iridum basin were identified by combining images, topography, spectrum data and dating result [2]. Except visible crater there are some craters/basins buried by basalts on lunar used to be called mascons. Mascons are kind of landform on lunar, mars and mercury which majorly studied by gravity data in the past. It was discovered in 1968, described as large positive gravity anomalies associated with the giant circular basins [3]. Science then, numerous Theories of relationship between mascons and mechanisms for creation of the circular basins has been suggested. Such as: mantle plugs upwelling into giant impact basins followed by volcanic filling [4, 5], puddling of high-density meteorite material [6], crater in a low-density lunar crust filled by normal-density basaltic lava[7], uplift of the basin center[8]…

 doi:10.20944/preprints202206.0051.v1

Before an improved gravity model from doppler tracking of the Lunar Prospector (LP) spacecraft come out, mascons known were all on the lunar nearside close to the equator and were filled with mare. The LP model help to identify seven new mascons around both sides of lunar, while three of them has no visible mare fill, improve the exist of mantle plug contribution [9]. Gravity Recovery and Interior Laboratory (GRAIL) lanched in 2011 return high resolution gravity data cause more discovery in mascons. The research was not limited to impact basins, but extended to buried basins. Scientists propose some new words refer to these small size mascons like quasi-circular mass anomalies (QCMAs) [10] and positive Bouguer gravity anomalies (PBGAs) [11]. With new 900 or 1200degree gravity model, more mascons have been identified. Evans et al. revealed more than 100 QCMAs on the lunar nearside and inferred a 1.5 km lower bound on the average thickness for the nearside lunar mare [10]. Two buried basins (200 km and 160 km in diameter) located in the northwestern rim of Lacus Somniorum and Maria Tranquillitatis validated the forward modeling approach [12]. Neumann et al. improves The GRAIL inventory of lunar basins twice more than earlier lists and determined the main ring diameters of previously known but degraded basins [13]. In Oceanus Procellarum, four PBGAs was recognized which also verify the inference of Evans et al [11]. GRAIL data also played an important role in clarifying the origin of mascons is caused by isostatic adjustment and cooling and contraction of a voluminous melt pool [8, 14-16]. However, most of these researches just based on gravity and topography data. Few of them bring in remote sensing images to prove their inference.

A buried basin to the south-eastern of Copernicus was given different diameter and classify as different types of basins [10, 13, 17]. Such case suggests that the current basin catalogs need further correction. As a result, in this paper gravity, images, topography and spectrum data are used to surveying the morphology feature and discuss the evolution of the buried basin.

2. Data and Methods

2.1. Datasets

In this study, we make use of high-resolution gravity field model of degree and order 1200 in spherical harmonics obtained by NASA's Gravity Recovery and Interior Laboratory mission (GRGM1200A) [18]. Moon LRO LOLA - SELENE Kaguya TC DEM Merge(59m/pixel) show the high-resolution topography [19]. Kaguya TCortho Mosaic Global image (7.4m/pixel) help to analysis the morphology and chronology of the buried basin. Olivine and optical maturity (OMAT) parameter images(59m/pixel) from Kaguya MI are also used [20]. Some olivine-bearing places such as Copernicus central peaks represent an olivine lithology occurring at depth [21] and high regional olivine contents might show the exitance of basalts in western mare [22]. OMAT is the degree to which a particular lunar soil possesses quantitative characteristics consistent with that exposure [23]. It shows the time that lunar surface expose to the space environment to distinguish type of surface. In addition, “Unified Geologic Map of the Moon, 1:5M, 2020” from NASA is used to learn the geology background of the research area [24]. Moon LRO LROC WAC Global Morphology Mosaic (100m/pixel) and Moon LROC WAC DTM GLD100(118m/pixel) are also used to display study area. Both of them are available through Astropedia (https://astrogeology.usgs.gov/site/annex).

2.2. Gravity

In this study, the field of Bouguer gravity data was truncated to degree and order 600 and derived from the GRAIL GRGM900C gravity model after subtracting the gravity resulting from topography assuming a density of 2500 kg/m3. Such processing aims of the expansion in the spatial domain and to highlight mid-to short-wavelength structure and reduce the effects of on remaining artifacts our analyses [10, 18, 25, 26]. The stretched renderer is adopted to display continuous pixel values across a gradual ramp

Preprints (www.preprints.org) | NOT PEER-REVIEWED | Posted: 6 June 2022 doi:10.20944/preprints202206.0051.v1

of colors and improve the display. Thus, mascons can be directly observed on Bouguer gravity data. Proposed basins may be recognized by their distinctive circular outlines in the Bouguer gravity map view [13]. For peak-ring basins the buried basin to the south-eastern of Copernicus belongs to, some features are helpful to recognize them: (1) Roughly circular rings although sometimes discontinuous. (2) A central positive Bouguer anomaly that is confined within the peak ring. (3) A negative Bouguer anomaly annulus that extends from the edge of the positive anomaly outward to the rim crest. (4) A number of degraded basins lacking interior peak rings have diameters and gravity patterns similar to those of well-preserved peak-ring basins [16].

2.3. Topography

In this paper, terrain analysis and morphologic analysis are introduced for the recognition of buried basins and its diameter. Terrain analysis based on DEM. On the edge of an impact basin there is a circle of raised rim which is usually the highest part of the basin. What's more, a ring of mountains first develops within the crater at about 140 km in diameter on the moon. The diameter of this inner "peak ring" is roughly half the crater rim diameter [27]. Rim and ring are the most visible characteristic of peak-ring basins on mosaic images. However, craters on lunar suffer from various mass-wasting processes and meteoroid bombardment. As a result, the rim height should decrease due to the downslope movement of rim and ejecta materials over time [28]. Furthermore, most part of basin rim and peak ring may disappear on the surface in the case of severe geological process.

As previous research suggests, some mascons surround by linear rilles or mare ridges are impact crater/basin filled by basalts [27]. Therefore, geological map is used to check if there are rilles or ridges around the mascon beside Copernicus.

2.4. Geochronology

Date of the buried basin was measured by crater size-frequency distribution (CSFD)[29]. This approach requires an accurate measurement of crater diameters within and well-defined geologic units [2]. The craters were mapped by "CraterTools", an ArcGIS plug-in [30]. With three evenly distributed points identified on the crater rims, the diameters would be accurate. Secondary craters which were distributed in chains, were excluded in the dating process [31]. Copernicus ejecta is from "Unified Geologic Map of the Moon, 1:5M, 2020" to eliminate the influence of the division of geological units. Resurfacing events may occur several times in the area and erase the relatively small craters. As a result, based on craters of different sizes, CSFD shows ages which correspond to different resurfacing events. For example, once a buried basin was resurfaced, the smallest group stands for the age of latest resurfacing event; middle group represents the time of basalts fill in, the largest group denotes the date of impact event. The dates of different events were fitted by both cumulative and differential fit using the Craterstats 2.0 tool, with the lunar chronology function (CF) and production function (PF) from Neukum (2001) [29].

2.5. Olivine Contents and OMAT

We search for a large enough fresh crater in the mascon to get outcrop and study underground layer. Olivine and OMAT from spectrum data suggest the nature of fill in material through outcrop. This may show the original surface of the buried basin. Then, the depth of buried basin can be estimated combined with DEM.

Lucey et al. provided algorithms to inverse OMAT based on Clementine UV/VIS images [22, 23].

$$OMAT = \left[(R_{750} - x_0)^2 + \left(\frac{R_{950}}{R_{750}} - y_0 \right)^2 \right]^2 \quad (1)$$

Preprints (www.preprints.org) | NOT PEER-REVIEWED | Posted: 6 June 2022 doi:10.20944/preprints202206.0051.v1

where x_0 is the reflectance of the origin, y_0 is the ratio value of the origin, R_{750} is the reflectance at 750 nm of a pixel or spectrum, and R_{950} is the reflectance at 950 nm of a pixel or spectrum. For Clementine data the constants are $x_0 = 0.08$ and $y_0 = 1.1$

In this study, the OMAT were derived from the Kaguya MI data. Thus, the regression coefficients described by Lemelin et al. [20] should be applied to the Multiband Imager data at 750 (R_{750}) and 950 (R_{950})nm in order to match the reflectance of Clementine at these bands ($R750_{corr}$, $R950_{corr}$).

$$R750_{corr} = (R_{750} * 1.51) + 0.020$$
$$R950_{corr} = (R_{950} * 1.38) + 0.020 \quad (2)$$

The method developed by Lemelin et al. use Hapke's radiative transfer equations and reflectance data from the Kaguya Multiband Imager are used to get the abundances of olivine [20].

3. Results

3.1. Bouguer Gravity Anomaly

The buried basin locates to the south-eastern of Copernicus. It has a typical positive Bouguer gravity anomaly and a negative Bouguer anomaly annulus that extends from the edge of the positive anomaly of masons as shown in Figure 1. The Bouguer gravity anomaly has a center at 7.42°N 17.87°W and 123km in diameter.

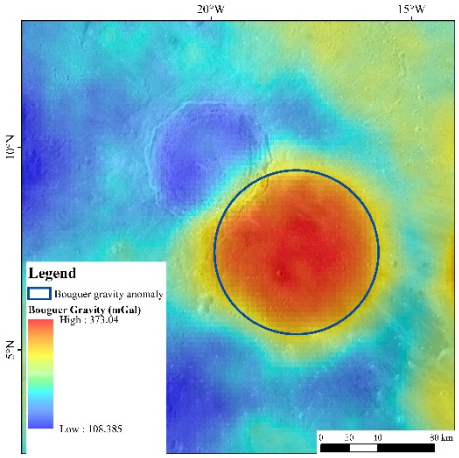

Figure 1. Bouguer gravity of Copernicus area.

3.2. Morphology and Topography

Some previous studies gave out diverse scale of the buried basin As Neumann et al. measured the mascon is a buried peak-ring basin has a center at 7.2°N 18.2°W, rim 260km in diameter and peak ring 130km in diameter [13] (blue circle in Figure 2). For Liu et al. the basin type and center are the same, but the rim is 483km in diameter and ring is 221km in diameter [17] (pink circle in Figure 2). Both of them are much larger than those of Neumann et al. Evans et al. measured the mascon as a single ring basin which located at 7.28°N 18.26°W and 175km in diameter (orange circles in Figure 2).[17].

Preprints (www.preprints.org) | NOT PEER-REVIEWED | Posted: 6 June 2022 doi:10.20944/preprints202206.0051.v1

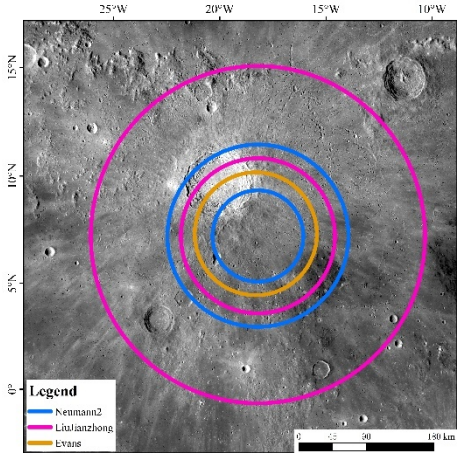

Figure 2. Previous studies results shown on LROC WAC Global Morphology Mosaic.

Most part of the basin rim and peak ring disappeared from lunar surface. However, at the north east part of Neumann's basin rim a surviving rim is visible in Figure 3. The surviving rim is only 20m higher than surrounding area.

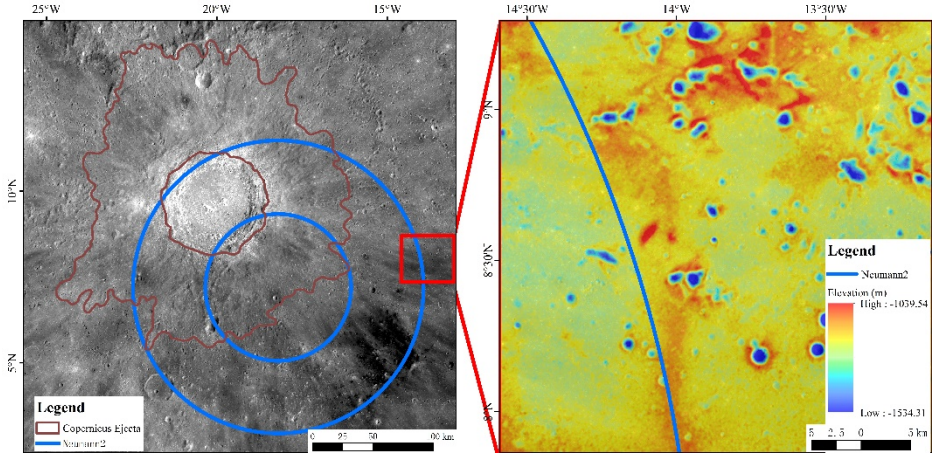

Figure 3. Surviving rim.

Solomon and Head [32] discovered that all mascon basins display an associated tectonic feature: linear rilles or mare ridges which tend to be concentric to the mascon. The buried basin matches this feature. There are rilles to the southwest and ridges to the southeast exhibited by red arrow in Figure 4.

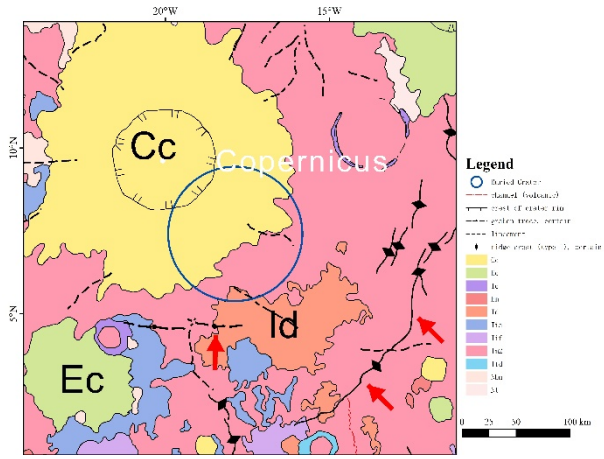

Preprints (www.preprints.org) | NOT PEER-REVIEWED | Posted: 6 June 2022 doi:10.20944/preprints202206.0051.v1

Figure 4. Geology map of Copernicus area.

3.3. Age

We pick the Bouguer gravity anomaly which is 123km in diameter and inside all three previous basin as the dating area to avoid different previous opinion about the scale of buried basin influence the dating result. 8848 small craters located in the buried basin were signed with a diameter range from 100m to 4500m (Figure 5(a)). 202 of them distributed in chains were recognized as secondary craters (Figure 5(a) yellow circle) and were rejected to eliminate error. The small size craters suggest age of surface ejecta and the large size craters shows age of the unit below ejecta [33]. In our experiment, craters between 160-400m gave 840Ma which represent the age of Copernicus (Figure 5(b)). Those between 700-3000m and 3200-4500m separately proved 3.4Ga and 3.6Ga (Figure 5(b)). In order to check the accuracy of dating result, we also signed craters on Copernicus ejecta. A similar age of 820Ma support the age of Copernicus. Both Copernicus ejecta dating results approach to the 800Ma isotope dating result [34, 35], suggest an accurate experiment result. Unit below the ejecta is 3.7Ga, a bit earlier than the buried basin, and shows a refresh event on the buried basin. Ages of units below ejecta belong to Imbrian. To allow for the Imbrian upper Mare unit (Im) located to southwest of Copernicus in Figure 4, units below ejecta might be Imbrian upper Mare unit.

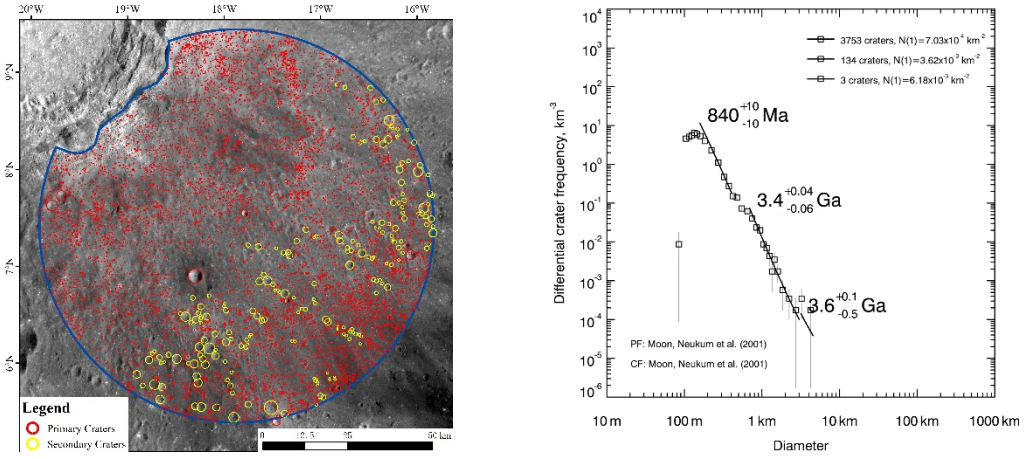

(**a**) (**b**)

Figure 5. Bouguer gravity anomaly CSFD dating.

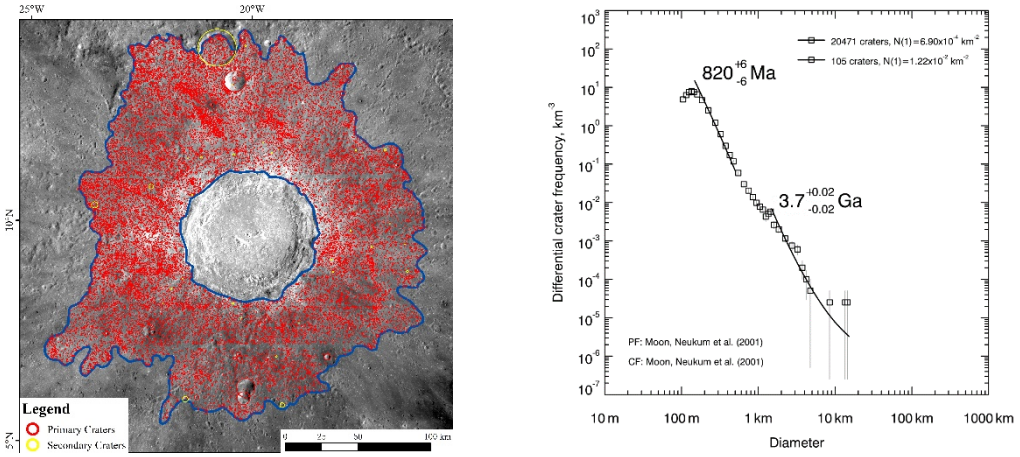

(**a**) (**b**)

Figure 6. Copernicus CSFD dating.

Preprints (www.preprints.org) | NOT PEER-REVIEWED | Posted: 6 June 2022 doi:10.20944/preprints202206.0051.v1

3.4. Mineral

Crater Copernicus H (Figure 7), a partial clue, gave an access to learn more about the buried basin. The fresh crater located at 6.89°N 18.29°W and 4.4km in diameter. Depth is 890m measured on LOLA - SELENE Kaguya TC DEM (Figure 8). The Profile indicate that Copernicus H is a flat-bottomed crater (Figure 8). Mineral maps from Kaguya MI images are used to study it. Both Olivine and OMAT map in Figure 9 demonstrate that the flat bottom has similar material but totally different from the crater rim wall. Geology map and CSFD dating help to identify the unit on the rim wall of Copernicus H is Im. This conforms to the high olivine content. Low olivine content and OMAT values of the flat bottom suggest a similar evolution process to the nowadays surface. Hence, Copernicus H is supposed to have penetrate the filled in material of the buried basin and expose the bottom of it.

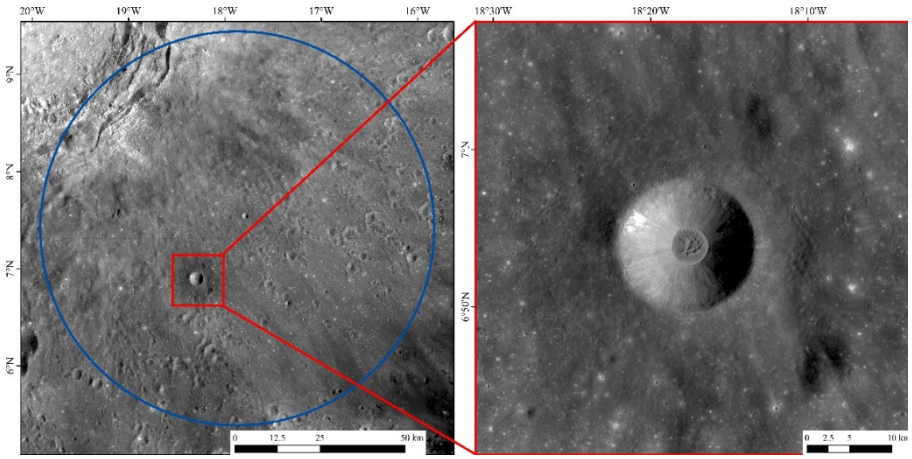

Figure 7. Position of Copernicus H crater.

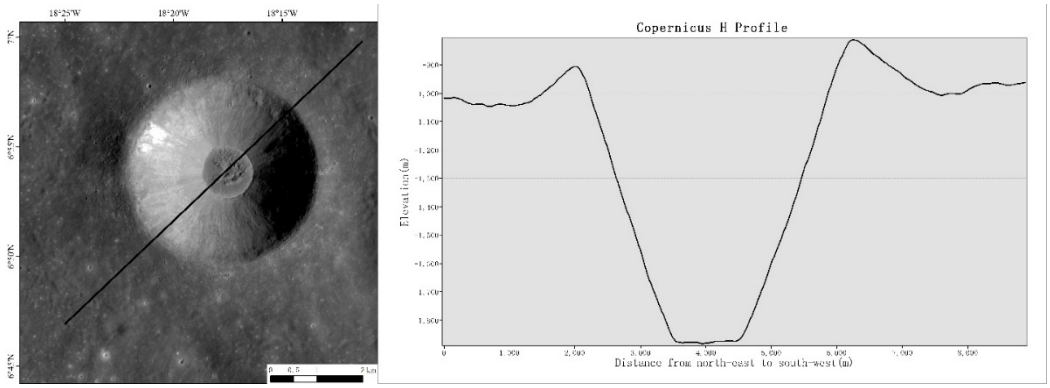

Figure 8. This is a figure. Schemes follow the same formatting.

Preprints (www.preprints.org) | NOT PEER-REVIEWED | Posted: 6 June 2022 doi:10.20944/preprints202206.0051.v1

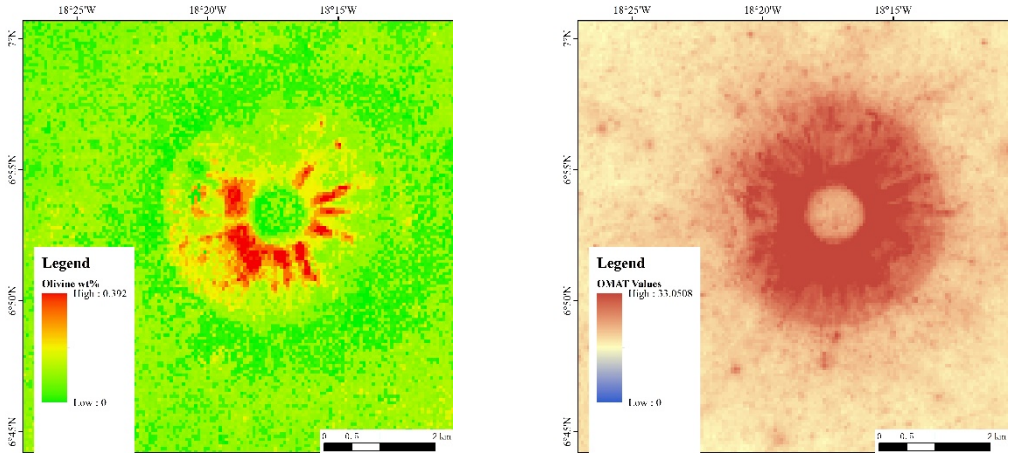

(a) (b)

Figure 9. Mineral maps of olivine and OMAT of Copernicus H.

Dark Mantling Deposit (DMD) Sinus Aestuum Ⅰ [36] locates on the south east part of the mascon. OMAT map shows that DMD has a low OMAT value than surrounding mare. This suggests that the DMD formed earlier than surrounding mare.

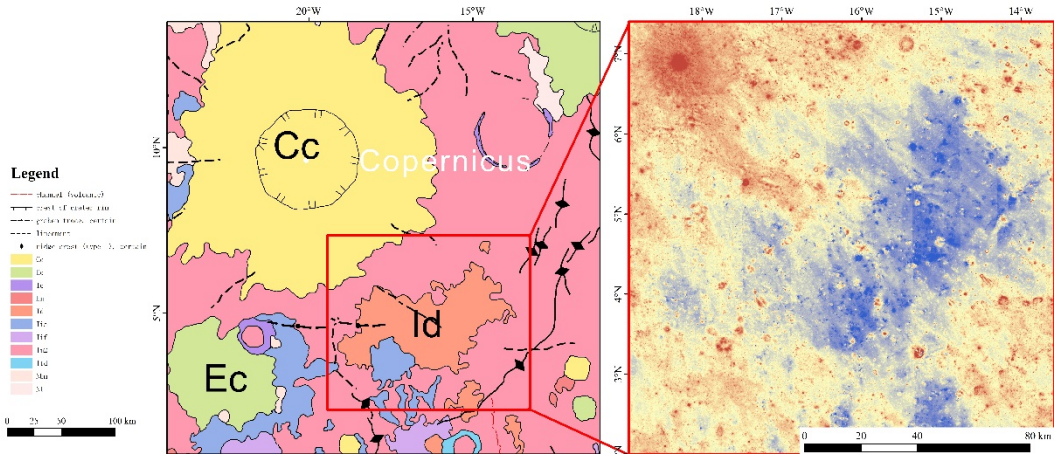

Figure 10. Position and OMAT map of DMD.

4. Discussion

4.1. Confirmation and characteristic of the buried basin

Because Neumann et al., Liu et al. and Evans et al. has quietly different conclusion on the scale and type of the buried basin, confirm the accurate scale and type becomes an important work. The mascon fit all the features of peaking-ring basin: (1) Roughly circular rings although sometimes discontinuous. (2) A central positive Bouguer anomaly that is confined within the peak ring. (3) A negative Bouguer anomaly annulus that extends from the edge of the positive anomaly outward to the rim crest. (4) A number of degraded basins lacking interior peak rings have diameters and gravity patterns similar to those of well-preserved peak-ring basins [16]. It should be classified into peak-ring crater. Liu et al. (pink circle in Figure 11) gave a much larger scale than Neumann et al. (blue circle in Figure 11). However, the rim given by Liu et al. overlay on the rim of Imbrium basin given by Neumann et al. (white circle in Figure 11). The topographic feature suggests that the highland north to Copernicus should belongs to the rim of Imbrium basin. In addition, Morphology and topography results in this paper shows a surviving rim which fit to the rim given by Neumann and the rim given by Liu et al. even goes be-

Preprints (www.preprints.org) | NOT PEER-REVIEWED | Posted: 6 June 2022 doi:10.20944/preprints202206.0051.v1

yond rilles and ridges surround the mascon. Thus, the buried basin can be confirmed that it located at 7.2°N 18.2°W, with rim 260km in diameter and peak ring 130km in diameter.

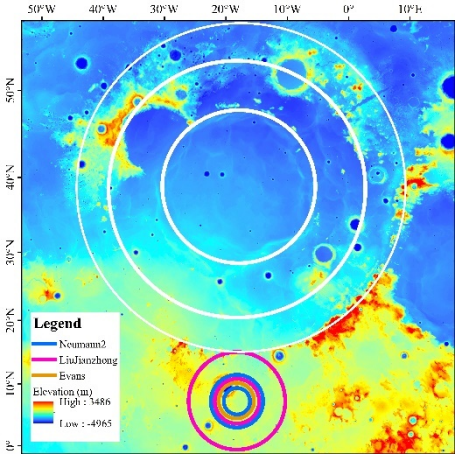

Figure 11. Previous studies results and Imbrium basin shown on LROC WAC DTM GLD100.

4.2. Thickness of Im in the buried basin

In mineral results part, topography (Figure 8) and spectrum (Figure 9) data analysis gets the 890m depth of Im. Research of Gong et al. [37] gives an access to identify our result. They used a localized multitaper spherical-harmonic analysis determined the thickness of mare basalts on the nearside lunar hemisphere from high-resolution gravity data acquired from GRAIL. But in their result different parameters combination leaded to widely different results. When the angular size of the window set θ=20° with 1σ upper bounds, the thickness value of the four measure points in Copernicus H are closest to ours. Kriging is adopted to get the thickness of Copernicus H from the four measure points and get a thickness of 930m. almost consistent with the 890m topography and spectrum analysis result. Furthermore, multi-source data combine analysis can help to determine the parameters of gravity mare thickness estimation.

4.3. Evolution of the buried basin

In CSDF dating of the buried basin, two ages (3.4 and 3.6Ga) comes out from large craters (Figure 5b). The low OMAT value in the flat bottom of Copernicus H shown by Figure 9b proves that the flat bottom exposes the original surface of the buried basin. Meanwhile, In Figure 9a, the rim wall of Copernicus has more olivine than the flat bottom suggests that basalts are above the original surface. Thus, 3.4Ga should correspond to the age of Im and 3.6Ga represent the impact event of the buried basin. This age is similar with the result of Liu et al. [17] The base rock forms earlier than 3.7Ga (Figure 6b). Considering Stadius crater (Figure 12) which located 186km east to Copernicus was obviously buried by Im, such assumption based on spectral and CSFD dating results is reasonable. Evans et al. divided QCMAs with diameters greater than 80km into high/low-relative-Bouguer-anomaly groups, interpreted as craters formed prior to and after the onset of local mare [10]. However, they didn't specify this characteristic of the buried basin in this paper. According to our assumption, the buried basin formed prior to Im and should be divided into high-relative-Bouguer-anomaly groups.

Preprints (www.preprints.org) | NOT PEER-REVIEWED | Posted: 6 June 2022 doi:10.20944/preprints202206.0051.v1

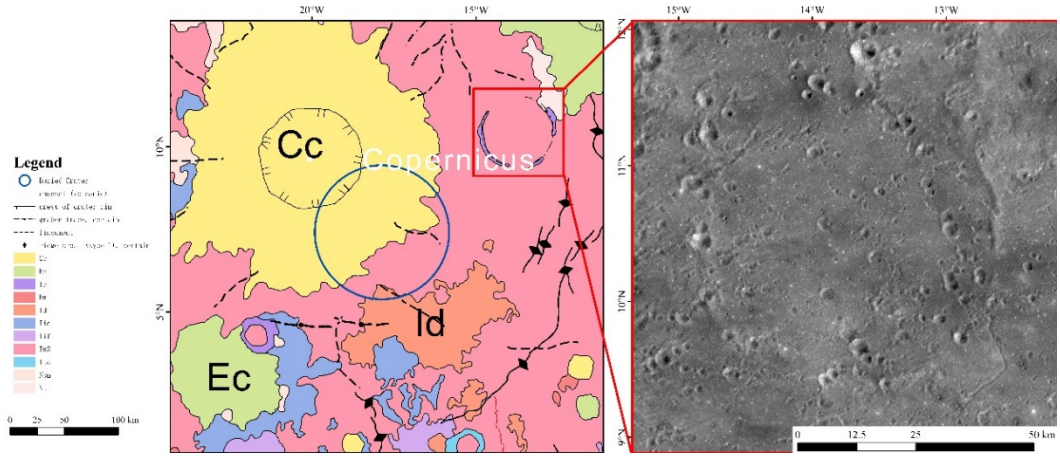

Figure 12. This is a figure. Schemes follow the same formatting.

The ages of Sinus Aestuum Ⅰ DMD (the Id part in Figure 12) cannot be obtained from CSFD because their unconsolidated nature is thought to have reduced artificially the number of small craters observed on their surfaces [38, 39]. Considering that Sinus Aestuum Ⅰ DMD has a lower OMAT value than the mare, the corresponding hawaiian-style eruption event should early than the formation of mare.

After joint the age of Copernicus, the evolution of the buried basin can be expressed as: An impact event occurred 3.6Ga ago. Then, a hawaiian-style eruption formed Sinus Aestuum Ⅰ DMD. In 3.4Ga, mantle plugs upwelling into giant impact basins followed by volcanic filling in Copernicus and nearby area forming the positive Bouguer gravity anomaly buried basin and Im units. Then ejecta from Copernicus impact event in about 820Ma and weathering processes cause the buried basin almost disappeared from lunar surface. Finally, Copernicus H exposed the original surface.

5. Conclusions

This section is not mandatory but can be added to the manuscript if the discussion is unusually long or complex.

We use multi source remote sensing data includes: images, topography, spectrum to analysis the positive Bouguer gravity anomaly to the south east of Copernicus. Our results show that the mascon (QCMA) is a buried basin. Details of the buried basin lead to the following conclusions:

1. The buried basin basic parameters are updated to located in 7.2°N 18.2°W, with rim 260km in diameter and peak ring 130km in diameter. in diameter and should be classified as peak-ring crater and divided into high-relative-Bouguer-anomaly groups.
2. DEM and spectral data in Copernicus H suggest that thickness of Im in the buried basin is 890. What's more，the angular size of the window set θ=20° with 1σ upper bounds are the best parameters for the localized multitaper spherical-harmonic method in Copernicus area.
3. The buried basin impact event occurred in 3.6Ga. Then, a hawaiian-style eruption formed Sinus Aestuum Ⅰ DMD. Im filled in it in 3.4Ga. Besides the intrusive basalts, ejecta from Copernicus impact event in about 820Ma and weathering processes also cause the disappearing from lunar surface of the buried basin.

Author Contributions: Conceptualization, X.X.; methodology, X.X. and T.H.; formal analysis, X.X. and T.H.; data curation, X.X., X.D., and L.Z.; writing- original draft preparation, X.X.; supervision, Z.K.; project administration, Z.K.; funding acquisition, Z.K. All authors have read and agreed to the published version of the manuscript.

Funding: This work was supported by National Key Research and Development project (2019YFE0123300).

Data Availability Statement: GRGM1200A bouguer data gggrx_1200l_boug_l660 are obtained from NASA's Planetary Data System (PDS): https://ode.rsl.wustl.edu/moon/indexDatasets.aspx. Moon LRO LOLA - SELENE Kaguya TC DEM Merge, olivine and optical maturity (OMAT) parameter images from Kaguya MI and Kaguya TCortho Mosaic Global image are available at https://astrogeology.usgs.gov/site/annex. Unified Geologic Map of the Moon, 1:5M, 2020 from NASA can be downloaded at https://astrogeology.usgs.gov/search/map/Moon/Geology/Unified_Geologic_Map_of_the_Moon. Moon LRO LROC WAC Global Morphology Mosaic can be downloaded at https://astrogeology.usgs.gov/search/map/Moon/LRO/LROC_WAC/Lunar_LRO_LROC-WAC_Mosaic_global_100m_June2013.cub. Moon LROC WAC DTM GLD100 can be downloaded at https://astrogeology.usgs.gov/search/map/Moon/LRO/LROC_WAC/Lunar_LROC_WAC_GLD100_79s79n_118m_v1_1.cub.

Acknowledgments: Not applicable.

Conflicts of Interest: The authors declare no conflict of interest.

References

1. Kang Z, Wang X, Hu T, et al. Coarse-to-Fine Extraction of Small-Scale Lunar Impact Craters From the CCD Images of the Chang'E Lunar Orbiters [J]. IEEE Transactions on Geoscience and Remote Sensing, 2019, 57(1): 181-193.
2. Hu T, Kang Z, Massironi M, et al. Geological evolution of the Sinus Iridum basin [J]. Planetary and Space Science, 2020, 194.
3. Muller P M, Sjogren W L. Mascons: Lunar Mass Concentrations [J]. Science, 1968, 161(3842): 680-684.
4. Wise D U, Yates M T. Mascons as structural relief on a lunar 'moho' [J]. Journal of Geophysical Research, 1970, 75(2).
5. Phillips R J, Dvorak J. The origin of lunar mascons: analysis of the Bouguer gravity associated with Grimaldi, F January 01, 1981, 1981 [C].
6. Urey H C. Mascons and the History of the Moon [J]. Science, 1968, 162(3860): 1408-1410.
7. Conel J E, Holstrom G B. Lunar Mascons: A Near-Surface Interpretation [J]. Science, 1968, 162(3860): 1403-1405.
8. Andrews-Hanna J C. The origin of the non-mare mascon gravity anomalies in lunar basins [J]. Icarus, 2013, 222(1): 159-168.
9. Konopliv A S, Binder A B, Hood L L, et al. Improved gravity field of the moon from lunar prospector [J]. Science, 1998, 281(5382): 1476-1480.
10. Evans A J, Soderblom J M, Andrews-Hanna J C, et al. Identification of buried lunar impact craters from GRAIL data and implications for the nearside maria [J]. Geophysical Research Letters, 2016, 43(6): 2445-2455.
11. Deutsch A N, Neumann G A, Head J W, et al. GRAIL-identified gravity anomalies in Oceanus Procellarum: Insight into subsurface impact and magmatic structures on the Moon [J]. Icarus, 2019, 331: 192-208.
12. Sood R, Chappaz L, Melosh H J, et al. Detection and characterization of buried lunar craters with GRAIL data [J]. Icarus, 2017, 289: 157-172.
13. Neumann G A, Zuber M T, Wieczorek M A, et al. Lunar impact basins revealed by Gravity Recovery and Interior Laboratory measurements [J]. Sci Adv, 2015, 1(9): e1500852.
14. Melosh H J, Freed A M, Johnson B C, et al. The Origin of Lunar Mascon Basins [J]. Science, 2013, 340(6140): 1552-1555.
15. Montesi L G J. Solving the Mascon Mystery [J]. Science, 2013, 340(6140): 1535-1536.
16. Baker D M H, Head J W, Phillips R J, et al. GRAIL gravity observations of the transition from complex crater to peak-ring basin on the Moon: Implications for crustal structure and impact basin formation [J]. Icarus, 2017, 292: 54-73.
17. Liu J, Liu J, Yue Z, et al. Characterization and interpretation of the global lunar impact basins based on remote sensing [J]. Icarus, 2022, 378.
18. Goossens S, Sabaka T J, Wieczorek M A, et al. High-Resolution Gravity Field Models from GRAIL Data and Implications for Models of the Density Structure of the Moon's Crust [J]. Journal of Geophysical Research: Planets, 2020, 125(2).
19. Barker M K, Mazarico E, Neumann G A, et al. A new lunar digital elevation model from the Lunar Orbiter Laser Altimeter and SELENE Terrain Camera [J]. Icarus, 2016, 273: 346-355.
20. Lemelin M, Lucey P G, Gaddis L R, et al. Global Map Products from the Kaguya Multiband Imager at 512 ppd: Minerals, FeO, and OMAT [Z]. 2016: 2994
21. Dhingra D, Pieters C M, Head J W. Multiple origins for olivine at Copernicus crater [J]. Earth and Planetary Science Letters, 2015, 420: 95-101.
22. Lucey P G. Mineral maps of the Moon [J]. Geophysical Research Letters, 2004, 31(8).
23. Lucey P G, Blewett D T, Taylor G J, et al. Imaging of lunar surface maturity [J]. J Geophys Res-Planet, 2000, 105(E8): 20377-20386.

24. Fortezzo C M, Spudis P D, Harrel S L. Release of the Digital Unified Global Geologic Map of the Moon at 1:5,000,000-Scale, F 2020/03/1].
25. Konopliv A S, Park R S, Yuan D-N, et al. High-resolution lunar gravity fields from the GRAIL Primary and Extended Missions [J]. Geophysical Research Letters, 2014, 41(5): 1452-1458.
26. Lemoine F G, Goossens S, Sabaka T J, et al. GRGM900C: A degree 900 lunar gravity model from GRAIL primary and extended mission data [J]. Geophys Res Lett, 2014, 41(10): 3382-3389.
27. Melosh H J. Impact cratering : a geologic process [M]. 1989.
28. Du J, Fa W, Wieczorek M A, et al. Thickness of Lunar Mare Basalts: New Results Based on Modeling the Degradation of Partially Buried Craters [J]. Journal of Geophysical Research: Planets, 2019, 124(9): 2430-2459.
29. Neukum G, Ivanov B A, Hartmann W K. Cratering Records in the Inner Solar System in Relation to the Lunar Reference System [J]. Space Sci Rev, 2001, 96(1): 55-86.
30. Kneissl T, van Gasselt S, Neukum G. Map-projection-independent crater size-frequency determination in GIS environments—New software tool for ArcGIS [J]. Planetary and Space Science, 2011, 59(11-12): 1243-1254.
31. Michael G G, Platz T, Kneissl T, et al. Planetary surface dating from crater size–frequency distribution measurements: Spatial randomness and clustering [J]. Icarus, 2012, 218(1): 169-177.
32. Solomon S C, Head J W. Lunar Mascon Basins: Lava filling, tectonics, and evolution of the lithosphere [J]. Reviews of Geophysics, 1980, 18(1): 107-141.
33. [33] Yue Z, Yang M, Jia M, et al. Refined model age for Orientale Basin derived from zonal crater dating of its ejecta [J]. Icarus, 2020, 346.
34. [34] Eberhardt P, Geiss J, Grögler N, et al. How old is the crater copernicus? [J]. The moon, 1973, 8(1): 104-114.
35. [35] Alexander E C, Jr., Bates A, Coscio M R, Jr., et al. K/Ar dating of lunar soils II [J]. Lunar and Planetary Science Conference Proceedings, 1976, 1: 625-648.
36. [36] Weitz C M, Head J W, Pieters C M. Lunar regional dark mantle deposits: Geologic, multispectral, and modeling studies [J]. Journal of Geophysical Research: Planets, 1998, 103(E10): 22725-22759.
37. [37] Gong S, Wieczorek M A, Nimmo F, et al. Thicknesses of mare basalts on the Moon from gravity and topography [J]. Journal of Geophysical Research: Planets, 2016, 121(5): 854-870.
38. [38] Gaddis L R, Staid M I, Tyburczy J A, et al. Compositional analyses of lunar pyroclastic deposits [J]. Icarus, 2003, 161(2): 262-280.
39. [39] Gustafson J O, Bell J F, Gaddis L R, et al. Characterization of previously unidentified lunar pyroclastic deposits using Lunar Reconnaissance Orbiter Camera data [J]. Journal of Geophysical Research: Planets, 2012, 117(E12): n/a-n/a.